Magnetic Resonance Materials in Physics, Biology and Medicine (2019) 32:123–132
https://doi.org/10.1007/s10334-018-0715-7

RESEARCH ARTICLE

Preclinical ^{19}F MRI cell tracking at 3 Tesla

Ashley V. Makela[1,2] · **Paula J. Foster**[1,2]

Received: 16 August 2018 / Revised: 6 October 2018 / Accepted: 27 October 2018 / Published online: 12 November 2018

Abstract

Purpose To develop methods for fluorine-19 (^{19}F) MRI cell tracking in mice on a 3 Tesla clinical scanner. Compared to iron-based cell tracking, ^{19}F MRI has lower sensitivity and, consequently, preclinical ^{19}F cell tracking has only been performed at relatively high magnetic field strengths (> 3 T). Here, we focus on using ^{19}F MRI to detect macrophages in tumors; macrophage density is an indication of tumor aggressiveness and, therefore, ^{19}F MRI could be used as an imaging biomarker.

Methods Perfluorocarbon (PFC)-labeled macrophages were imaged at 3 T and NMR spectroscopy was performed to validate ^{19}F spin quantification. In vivo ^{19}F MRI was performed on tumor-bearing mice, post-PFC at both 9.4 T and 3 T. 3 T MRI utilized varying NEX and ^{19}F images were analyzed two different ways for ^{19}F quantification.

Results As few as 25,000 cells could be detected as cell pellets at 3 T. ^{19}F quantification in cell pellets by 3 T MRI agreed with NMR spectroscopy. ^{19}F signal was observed in the liver, spleen and tumor in all mice at 9.4 T and 3 T and there was no significant difference in ^{19}F spin quantification.

Conclusion This study demonstrates the ability to detect and quantify ^{19}F signal in murine tumors using ^{19}F MRI at 3 T.

Keywords 19-Fluorine (^{19}F) · Magnetic resonance imaging (MRI) · Cancer · Cell tracking · Tumor-associated macrophage (TAM)

Introduction

Fluorine-19 (^{19}F)-based magnetic resonance imaging (MRI) has recently become an attractive method to image cells in vivo in preclinical studies. This is due to its inherent specificity, quantification ability and chemical inertness of the agent administered. For these reasons, ^{19}F MRI has been used in many different experimental cell tracking studies including, for example, imaging of immune cells in arthritis [1], bowel disease [2], experimental autoimmune encephalomyelitis [3] and cancer [4–7]. However, compared to the more widely used iron-based MRI, ^{19}F is much less sensitive. Limiting factors which contribute to sensitivity have been thoroughly discussed by Srinivas et al. [8] and include the amount of fluorine which can be delivered to a region of interest (i.e., ^{19}F concentration [9], due to cell loading and/or number of ^{19}F spins on the label), MR properties of the ^{19}F label, MRI system and MRI acquisition parameters. One or a combination of these factors may result in low signal to noise (SNR) which could impair ^{19}F detection. To compensate, it is common to image at a high magnetic field strength to increase ^{19}F signal. Another simple approach for increasing sensitivity is to use multiple acquisitions, or signal averages, which are summed for improved SNR—this requires longer scan times. All in vivo preclinical ^{19}F MRI cell tracking studies have been performed at field strengths above 3 Tesla (T) and have used multiple acquisitions [1, 10–15].

We have previously used ^{19}F MRI at 9.4 T to demonstrate the ability to detect and quantify tumor-associated macrophages (TAMs) in a preclinical model of breast cancer [5]. TAM presence and number have been shown to be correlated to breast tumor aggressiveness including growth, progression, metastasis and clinical outcome [16–18]. Our study showed that tumors with different levels of aggressiveness could be distinguished using ^{19}F MRI cell tracking. The ability to detect and monitor the number of TAMs in individual tumors with ^{19}F MRI could allow for identification of breast tumors with heavy infiltration of TAMs and could

✉ Ashley V. Makela
amakela@uwo.ca

[1] Robarts Research Institute, London, ON, Canada

[2] The Department of Medical Biophysics, Western University, 1151 Richmond Street North, London, ON N6A 5B7, Canada

be used as a biomarker for decisions about how to best treat these patients as well as for monitoring responses to therapy.

The translation of cellular MRI techniques to the clinic will require the use of human MRI systems, the maximum field strength of which is presently 3 T, in most places. In this paper, we begin to explore the feasibility of performing ^{19}F MRI cell tracking at 3 T in a murine model. We show that ^{19}F-labeled cells can be detected in vivo in mice using a clinical 3 T MRI system.

Methods

Cell culture

4T1 murine breast cancer cells (Dr. Fred Miller, Wayne State University, MI, USA) and RAW264.7 murine macrophages (Dr. Greg Dekaban, Western University, ON, CAN) were maintained at 37 °C and 5% CO_2 in Dulbecco's Modified Eagle's Medium–high glucose media [4T1 (Thermofisher, ON, CAN)] and RPMI [RAW264.7 (Thermofisher, ON, CAN)] supplemented with 10% fetal bovine serum, penicillin/streptomycin (4T1 and RAW264.7) and L-Glutamine, HEPES, beta-mercaptoethanol [RAW264.7 (Thermofisher, ON, CAN)]. Cells were passaged every 2–3 days (4T1) and 3–4 days (RAW264.7).

In vitro cell labeling

RAW264.7 murine macrophages were labeled with a perfluoropolyether perfluorocarbon (PFC) agent (V-Sense, VS-1000H or a red fluorescent-tagged version, VS-1000H DM Red, CelSense Inc., Pittsburgh, USA). Labeling took place over ~ 24 h at a concentration of 2.5 mg/ml. Cells were washed 3 times with PBS followed by trypsinization. A 10 µl sample was diluted 1:1 with trypan blue and was used for cell counting and viability (Countess Automated Cell Counter; Invitrogen, Carlsbad, CA, USA). PFC-labeled macrophage pellets were then spun down in an Eppendorf tube, supernatant removed, and topped with 1% agarose for MRI or prepared for NMR spectroscopy (see below).

Animal model

Female BALB/c mice (6–7 weeks; Charles River Canada) were obtained and cared for in accordance with the standards of the Canadian Council on Animal Care, under an approved protocol by the Animal Use Subcommittee of Western University's Council on Animal Care. Mice were anesthetized with isoflurane administered at 2% in oxygen prior to receiving an injection of 300,000 4T1 cells (> 90% viability, measured using the trypan blue exclusion assay) suspended in 50 µl Hanks balanced salt solution (HBSS) into the 4th inguinal mammary fat pad, as previously reported [19, 20]. Animals were observed until alert and active, when they were returned to their cages.

In vitro MRI at 3 T and NMR spectroscopy

Two separate sets of PFC-labeled murine macrophage pellets with high numbers of cells [25, 50, 75, 125, 250, 500, 750 ($\times 10^3$), 1, 1.5, 2 and 5 ($\times 10^6$) cells] and low numbers of cells [5, 10, 25, 125 and 250 ($\times 10^3$) cells] were imaged to evaluate the minimum number of cells that could be detected at 3 T. Images were acquired using a clinical GE 3 T MR750 system (General Electric, ON, CAN) and a 4.3 × 4.3 cm dual tuned ^{1}H/^{19}F surface coil (Clinical MR Solutions, WI, USA). This coil was originally built for imaging small ROIs on humans. ^{1}H images were acquired with a 2D fast gradient echo sequence with the following parameters: field of view (FOV) = 50 × 50 mm, matrix = 256 × 256, slice thickness = 5 mm, TR/TE = 100/4.9 ms, flip angle (FA) = 20°, bandwidth (BW) = ± 31.25 kHz, number of signal averages (NEX on a GE scanner) = 4 and scan time = 3.5 min. ^{19}F images were acquired using a 3D balanced steady-state free precession (bSSFP) sequence with 1 mm^3 spatial resolution, FOV = 50 × 50 mm, matrix = 50 × 50, slice thickness = 1 mm, TR/TE = 5.7/2.7 ms, FA = 72°, BW = ± 10 kHz, NEX = 60 and scan time = 30 min.

In a separate experiment, cell pellets containing 450,000 and 900,000 PFC-labeled murine macrophages were used to compare the quantification of ^{19}F spins using 3 T MRI and NMR spectroscopy. For MRI, there were 3 cell pellets containing 450,000 cells and 3 cell pellets containing 900,000 cells. These were imaged together using the same parameters as above. The samples were imaged 4 times, each time with a different number of NEX: 10, 20, 40 or 80 NEX.

For NMR of PFC-labeled cells, 3 samples containing 450,000 cells and 3 samples containing 900,000 cells were lysed with 10 µl RIPA buffer (VWR, Mississauga, CAN) and sonicated followed by 3 freeze–thaw cycles. This lysate was placed in an NMR tube with 0.1% trifluoroacetic (TFA) acid and D_20. All ^{19}F NMR measurements were performed at 376.12 MHz using a Varian Inova 400 spectrometer (Varian Inc, Palo Alto, USA). Spectroscopy parameters were: recycle delay = 6 s, acquisition time = 1 s, spectral width = 18.9 kHz (− 102 ppm to − 62 ppm), tip angle = 60°, number of scans = 100 and scan time = 13 min. The mean intracellular ^{19}F per cell was calculated from the ratio of the integrated areas of the PFC and TFA spectra.

In vivo MRI

Mice bearing 4T1 tumors at 3 weeks post-implantation were administered 200 µl of the PFC agent intravenously (IV) via the tail vein 24 h prior to imaging. While imaging,

mice were anesthetized with 2% isoflurane in oxygen. Two cell pellets containing 1 and 2 ($\times 10^6$) PFC-labeled macrophages and two reference tubes of known ^{19}F concentration (3.33×10^{16} ^{19}F/μl) were placed alongside the mice for quantification purposes (see below). Mice ($n = 2$) were imaged with ^{1}H and ^{19}F first on a small animal 9.4 T MRI (Varian Inc., Palo Alto, USA) using a custom built dual ^{1}H/^{19}F birdcage coil with a 3 cm diameter and then immediately after at 3 T. In vivo ^{1}H and ^{19}F images were both acquired with 3D bSSFP pulse sequences.

At 9.4 T, ^{1}H imaging parameters were: 500 μm^3 spatial resolution, FOV = 80 × 40 mm, matrix = 160 × 80, slice thickness = 0.5 mm, FA = 20°, BW = ± 62.5 kHz, TR/TE = 2.9/1.5 ms, 4 signal averages and 8 phase cycles (PC) with a scan time of 10 min. ^{19}F imaging parameters were: 1 mm^3 spatial resolution, FOV = 80 × 40 mm, matrix = 80 × 40, slice thickness = 1 mm, FA = 63°, BW = ± 25 kHz, TR/TE = 3.1/1.6 ms, 4 signal averages and 30 PC resulting in a scan time of 30 min.

At 3 T, ^{1}H imaging parameters were: 0.5 × 0.5 × 0.6 mm spatial resolution, FOV = 80 × 40 mm, matrix = 160 × 80, slice thickness = 0.6 mm, FA = 35°, BW = ± 31.25 kHz, TR/TE = 6.3/3.2 ms, 6 NEX and 8 PC with a scan time of 35 min. ^{19}F imaging parameters were: 1 mm^3 spatial resolution, FOV = 80 × 40 mm, matrix = 80 × 40, slice thickness = 1 mm, FA = 72°, BW = ± 10 kHz, TR/TE = 5.6/2.8 ms and 100 NEX resulting in a scan time of 30 min.

Using a separate group of tumor-bearing mice ($n = 4$), consecutive ^{19}F images were acquired at 3 T using 2, 5, 10, 19, 38, 75 and 150 NEX (resulting in 0.5, 1, 2, 4, 8, 16, 30 min scans). ^{1}H parameters were: 200 μm^3 spatial resolution, FOV = 70 × 35 mm, matrix = 350 × 175, slice thickness = 0.2 mm, FA = 20°, BW = ± 31.25 kHz, TR/TE = 11.9/5.9 ms, 1 NEX and 4 phase cycles with a scan time of 25 min and ^{19}F images were acquired with the above 3 T parameters with an FOV = 70 × 35 mm and matrix = 70 × 35.

Histological analysis

Mice were euthanized via overdose of isoflurane following the last MRI exam. Mice were transcardially perfused with saline followed by 4% paraformaldehyde. All primary tumors were excised and cryoprotected by passaging through a sucrose gradient of 10, 20, and 30% for 24 h each. Samples were then frozen in optimal cutting temperature compound and cryostat sections were collected (10 μm). Tumor tissue was examined using fluorescence microscopy to detect the Texas Red fluorescence of the PFC and subsequently stained using rat anti-mouse F4/80 primary antibody (Bio-Rad AbD Serotec Inc., Raleigh, NC, CI:A3-1, MCA497) to identify macrophages.

A sample of the PFC-labeled macrophages containing ~ 300,000 cells in ~ 300 μl PBS was centrifuged to make cells adhere to a slide. After fixation, slides were stained with nuclear fast red to enhance visualization of the PFC droplets with bright field microscopy.

Microscopy was performed using a Zeiss Axio Imager A1 microscope (Zeiss Canada, Toronto, ON, Canada) equipped with a Retiga EXi (QImaging Scientific Research Cameras, Surrey, BC, Canada) digital camera.

Analysis of MRI data

^{19}F images were overlaid onto the ^{1}H images (Osirix, Pixmeo SARL, Bernex, Switzerland) for anatomical reference of the ^{19}F signal within either the macrophage pellets or mice. Manual ROI delineation for ^{19}F quantification was performed in two different ways: (1) By choosing only voxels which are judged to contain ^{19}F signal in each pellet or tumor, after a window/level algorithm is applied ("^{19}F only" ROI) and (2) By outlining a tumor slice by slice in the ^{1}H images, creating a whole tumor 3D ROI and then copying the ROI onto the ^{19}F images ("tumor" ROI).

Average magnitude ^{19}F signal from the tumors (using "tumor" and "^{19}F only" ROIs) or pellets and reference tubes (S) and standard deviation of the noise (σ) were obtained from each data set to calculate SNR $\left(\text{SNR} = 0.655 \times \frac{S}{\sigma}\right)$ of tumors or pellets.

In brief, the total number of ^{19}F spins was determined by comparing the total ^{19}F signal within a chosen ROI to the signal generated by a reference tube containing a known amount of ^{19}F spins (3.33×10^{16} ^{19}F/μl). It is known that in low SNR situations there is a rician distribution of signal in the noise [21]. Many of these data sets will have low SNR due to low NEX, so therefore when tumor or pellet SNR < 5, a correction of 0.655 was made to the magnitude signal before calculating ^{19}F spins, as described previously [14].

Statistical analysis

Statistical analyses were performed using PRISM software (Graphpad, Version 7.0a). To compare the number of ^{19}F spins quantified from MR images and the known cell number in the PFC-labeled macrophage pellets, the Pearson correlation coefficient was used. A one-way ANOVA was performed to determine differences in ^{19}F quantification by NMR and all MRI exams (80, 40, 20, 10 NEX). A paired, two-tailed t test was used to compare ^{19}F quantification between 9.4 T and 3 T MRI exams.

Results

In vitro ^{19}F quantification at 3 T MRI and NMR spectroscopy

PFC-labeled murine macrophages imaged at 3 T showed that the ^{19}F signal from pellets containing as few as 25,000 cells could be detected. No ^{19}F signal was detected from the pellets containing 5000 or 10,000 cells (not shown). PFC-labeled macrophage pellets were visible as a homogeneous region of ^{19}F signal. A ^{1}H/^{19}F overlay from the "high number" PFC-labeled cell pellets is shown in Fig. 1a. Low signal is visualized in 75, 50 and 25 ($\times 10^3$) cell pellets in the single image slice shown in Fig. 1a; however, there was additional signal in adjacent slices and a sagittal view of the 25,000 pellet (inset) demonstrates more obvious ^{19}F signal. A linear correlation was found between the known cell number in each pellet and the number of ^{19}F spins ($R=0.983$, $p<0.0001$) (Fig. 1b). A nuclear fast red stained cytospin slide containing a sample of PFC-labeled cells is shown in Fig. 1c and the PFC droplets can be clearly seen within cells. The average number of ^{19}F spins/cell as estimated from this experiment is 7.93×10^{11}.

Figure 2 shows the average number of ^{19}F spins determined by NMR spectroscopy and by 3 T MRI for PFC-labeled cell pellets containing 450,000 and 900,000 macrophages. The mean number of ^{19}F spins measured by NMR was 9.76×10^{16} for the six pellets containing 450,000 cells and 1.87×10^{17} for the six pellets containing 900,000 cells. From these data, the mean number of ^{19}F spins/cell was calculated as 2.12×10^{11}. The average number of ^{19}F spins determined by MRI was not significantly different ($p=0.9991$) from that measured by NMR, regardless of the NEX. Average pellet SNR was 5.89 for the six pellets containing 900,000 cells and 4.57 for the six pellets containing 450,000 cells. Mean ^{19}F spins/cell was calculated as 1.97×10^{11} by MRI.

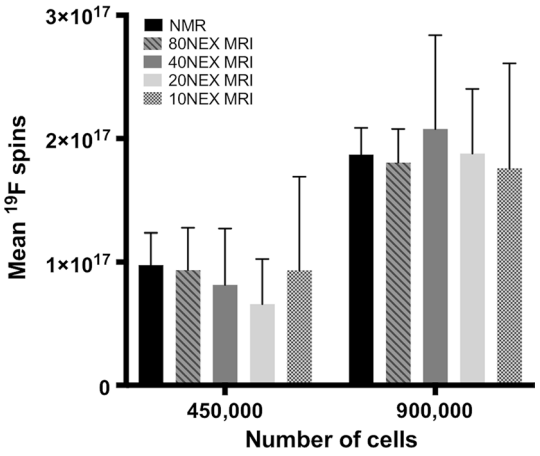

Fig. 2 In vitro PFC-labeled macrophages quantified by ^{19}F MRI (using varying NEX) and NMR. PFC-labeled macrophages (450,000 or 900,000 cells) were quantified by either MRI ($n=6$) using 80, 40, 20 and 10 NEX or NMR ($n=6$). There was no statistically significant difference in the mean number of ^{19}F spins measured by NMR versus MRI using the different MRI acquisitions ($p=0.9991$). The average ^{19}F/cell was 1.97×10^{11} by MRI and 2.12×10^{11} by NMR. MRI scan times were: 80 NEX = 18:05 min, 40 NEX = 9:03 min, 20 NEX = 4:32 min and 10 NEX = 2:08 min

Comparing in vivo mouse body ^{19}F MRI at 9.4 T and 3 T

Figure 3 shows 9.4 T (Fig. 3a) and 3 T (Fig. 3b) images of the same 4T1 tumor-bearing mouse, acquired ~ 24 h post-IV PFC. ^{19}F signal was observed in the liver, spleen, and tumor in both mice. In the representative image slice shown in Fig. 3, ^{19}F signal is visible in the liver and in the periphery of the tumor (as well as in the cell pellets included in the FOV).

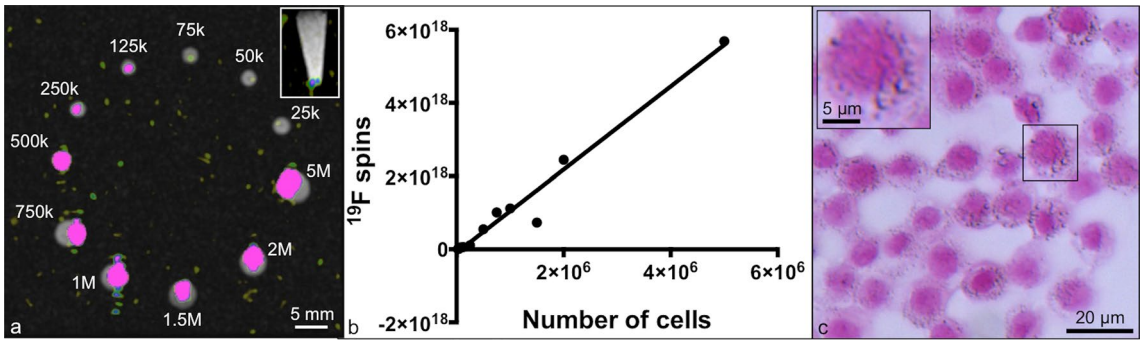

Fig. 1 ^{19}F MRI of in vitro PFC-labeled murine macrophages at 3 T. **a** ^{1}H/^{19}F MRI overlay of 25,000–5,000,000 PFC-labeled macrophage pellets. This ^{19}F image acquisition used 60 NEX resulting in a 30 min scan. ^{19}F signal detection limit was 25,000 cells (inset: sagittal image of 25,000 cell pellet). **b** ^{19}F spin quantification is linearly correlated with number of cells ($R=0.983$, $p<0.0001$) and average ^{19}F/cell calculated is 7.93×10^{11}. **c** PFC droplets can be seen in cells stained with nuclear fast red, without a marker under bright field microscopy (inset: zoomed). *k* thousand, *M* million

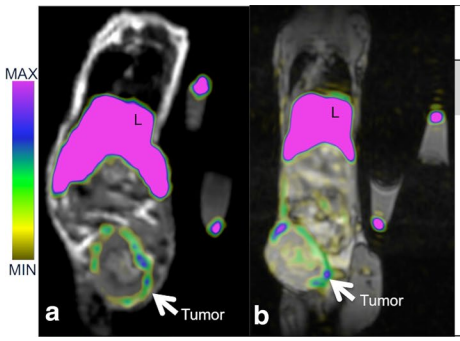

Number of ^{19}F spins

		3T	9.4T
Mouse A	Tumor	1.36×10^{19}	1.85×10^{19}
	Liver	1.53×10^{20}	1.96×10^{20}
Mouse B	Tumor	1.64×10^{19}	1.58×10^{19}
c	Liver	1.69×10^{20}	1.84×10^{20}

Fig. 3 ^{19}F MRI at 9.4 T and 3 T of a 4T1 tumor-bearing mouse. ^{1}H/^{19}F MRI overlays of the same 4T1 tumor-bearing mouse (Mouse A) at **a** 9.4 T and **b** 3 T, imaged consecutively. **c** There was no statistically significant difference in the number of ^{19}F spins measured for the tumor or liver, at 3 T versus 9.4 T, for each mouse. Using the value of ^{19}F/cell obtained from NMR of cell pellets (2.12×10^{11} ^{19}F/cell), an estimate of the number of PFC-labeled cells in this tumor is 64×10^{6} from 3 T or 87×10^{6} from 9.4 T. This analysis used the "tumor" ROI method. Reference tubes are not visible in these slices. *L* liver

The ^{19}F signal appeared similar in both the 9.4 T and 3 T images and the average tumor SNR at 9.4 T (10.6) and 3 T (7.9) was not significantly different between the MRI exams at different field strengths; ($p=0.7126$). The table presented in Fig. 3c describes the number of ^{19}F spins quantified in the tumor and liver for each mouse at 3 T and 9.4 T, using "tumor" ROI for ^{19}F quantification. The tumor and liver ^{19}F spin values are not significantly different when imaged at 3 T or 9.4 T ($p=0.5828$ and $p=0.2911$, respectively). If we use the value for ^{19}F/cell obtained from NMR, we can estimate that there is an average of 4.05×10^{7} PFC-labeled cells in a 4T1 tumor and 8.28×10^{8} PFC-labeled cells in the liver of these mice.

In vivo ^{19}F quantification at 3 T MRI

A window/level algorithm was applied to all ^{19}F images to enhance visualization of the tumor signal. In Fig. 4, representative images of the full dynamic range of signal in the whole mouse body are compared to the adjusted signal for visualization of tumor with high and low SNR acquisitions (150 NEX and 10 NEX, respectively). The relative minimum/maximum values of signal intensity for each image are included in figure legends.

Figure 5 shows a ^{1}H image of a tumor-bearing mouse along with ^{19}F images acquired with decreasing NEX/scan time, using "tumor" (Fig. 5a) and "^{19}F only" (Fig. 5b) ROIs. Examples of ROIs used for each are drawn over the tumor in white, in the ^{19}F images. The ROI volumes measured for this representative mouse are shown above each tumor; this is the ROI volume used for ^{19}F spin quantification. ^{19}F signal was detectable in the tumor, liver, spleen and reference tubes in all exams.

When using the "tumor" ROI (where the entire tumor was outlined), the same ROI was applied to every ^{19}F image (Fig. 5a). In the ^{19}F images, there is an obvious increase in noise as NEX/SNR decreases, when window/level values are the same in all images.

When using the "^{19}F only" ROI (where only obvious ^{19}F signal within the tumor was outlined), the size of the ROI chosen was different for each image acquired with different NEX. Window/level values were changed for each scan to optimize the visible ^{19}F signal in the tumor. ROI size increased as NEX/SNR increased because the ^{19}F signal was more obvious with less background noise. The quantification of ^{19}F spins from these two analysis methods is shown in Fig. 6.

In Fig. 6, scatter plots show the number of ^{19}F spins measured for each tumor, from each of the different acquisitions, using either the "tumor" ROI (Fig. 6a) or "^{19}F only" ROI (Fig. 6b) method. The average number of ^{19}F spins measured for each tumor, regardless of NEX, was similar for each analysis method. There was a smaller range of values for the number of ^{19}F spins measured for the different NEX when using a "tumor" ROI compared to the "^{19}F only" ROI. When using the "^{19}F only" ROI, there was a trend of higher numbers of ^{19}F spins measured with higher NEX.

Microscopy was used to confirm the presence of F4/80+ macrophages [brown staining, revealed by diaminobenzidine (DAB)] and the red fluorescent PFC agent. Figure 7 shows an example of a 4T1 tumor, 3 weeks post-cancer cell implantation, taken at the tumor periphery. The brown F4/80+ cells (Fig. 6a, d) correspond with the location of the red fluorescence from the PFC agent (Fig. 6b, e). Overlays (Fig. 6c, f) demonstrate that the location of the F4/80+/PFC+ cells correlates well with the ^{19}F signal, which is in the outer periphery of the tumor in the MR images in Fig. 3.

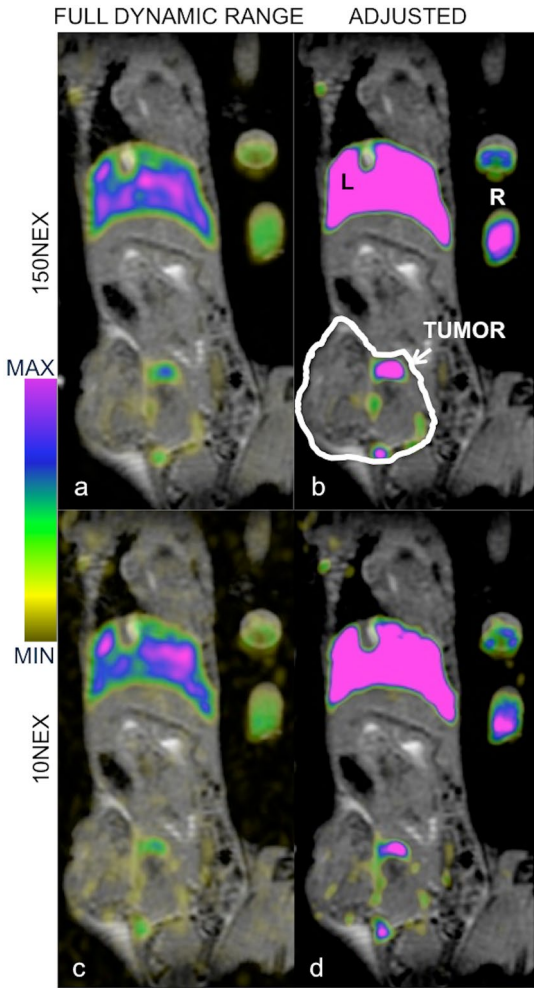

Fig. 4 $^{1}H/^{19}F$ MRI overlays of a 4T1 tumor-bearing mouse, showing the full dynamic range and adjusted ^{19}F signal at 3 T. Images were acquired with 150 and 10 NEX. Full dynamic range presents all signal intensities in each slice as lowest = yellow and highest = pink. There is a smaller window width in the adjusted images used to visualize the ^{19}F signal in the tumor (outlined in white) which does not represent all signal intensities. Minimum/maximum signal intensities: **a** 0/765, **b** 103/353, **c** 0/725, and **d** 109/375. *L* liver, *R* reference tubes

Discussion

This study demonstrates the use of a clinical 3 T MRI to image and quantify PFC-labeled cells in a preclinical murine model of breast cancer. We first used in vitro PFC-labeled macrophages to validate ^{19}F quantification by MRI and NMR. For in vivo studies, we analyzed the ^{19}F images two different ways, as we believe that there may be some user bias when manually delineating ^{19}F voxels with obvious signal ("^{19}F only" ROI), especially at a lower SNR with increased noise. When using a "tumor" ROI, where ROIs from anatomical images are placed onto ^{19}F images, this bias may be eliminated. Here, we used a range of number of NEX (resulting in a range of SNR), with ^{19}F spin number remaining more consistent when using "tumor" ROI versus "^{19}F only" ROI.

Cellular MRI is a powerful tool to track cells in vivo. Groups have used the IV administration of a cell label and subsequent MRI to track immune cells in vivo, overtime at multiple time points to evaluate the dynamics of cell infiltration [22] and response to treatments or interventions [1]. This technique relies on the labeling of macrophages in situ, including macrophages which are part of the reticuloendothelial system (i.e., liver, spleen, bone marrow, lymph nodes) [23–26]. Additionally, macrophages associated with cancer have been shown to take up both ^{19}F [4, 5, 27–29] and iron [30–32] agents. The advantage of cell tracking with ^{19}F MRI is the ability to quantify the signal; ^{19}F signal intensity is directly proportional to the amount of ^{19}F spins present in an ROI. When cells are labeled in vitro, cell loading can be determined by NMR and ^{19}F signal can be related to cell number. When cells are labeled in vivo, ^{19}F signal can be linearly related to a degree of inflammatory cell presence [33].

We first used in vitro PFC-labeled macrophage cell pellets to validate ^{19}F quantification and to get an estimate of ^{19}F spins/cell. ^{19}F MRI of cell pellets at 3 T showed a strong correlation between the number of cells in a pellet and the number of ^{19}F spins. A relatively low labeling concentration of 2.5 mg/ml (similar to other published methods [15, 34]) resulted in an estimate of 7.93×10^{11} ^{19}F spins/cell. From another sample of PFC-labeled cells, an estimate of 2.04×10^{11} ^{19}F spins/cell was obtained from MRI (using 80, 40, 20 and 10 NEX) and an average 2.12×10^{11} ^{19}F spins/cell was calculated by NMR. The lowest number of PFC-labeled cells detected by MRI at 3 T was 25,000, or 8.2×10^{15} ^{19}F spins.

We then examined the use of ^{19}F MRI at 3 T to track immune cells in vivo. In 3 T images of 4T1 tumor-bearing mice, 24 h post-PFC injection, we observed ^{19}F signal in the liver, spleen, tumor and reference tubes. We were able to quantify the number of ^{19}F spins in each 4T1 tumor. The average value for ^{19}F spins measured in 4T1 tumors at 3 T was 9.5×10^{18}, with the spatial distribution of ^{19}F signal around the tumor periphery, which agrees with our previous findings; that study was performed at 9.4 T [5]. The accumulation of TAMs and subsequent ^{19}F signal is sometimes referred to as "hot spots" [28]. Macrophages have been identified by multiphoton microscopy to localize as clusters in the periphery, or the "invasive edge", and their role here is to allow for tumor expansion and to aid in tumor cell intravasation [35, 36].

For mice imaged at both 3 T and 9.4 T, the number of ^{19}F spins measured in liver and tumor was not significantly different between the two magnetic field strengths. Despite the higher magnetic field strength, ^{19}F SNR was only slightly higher at 9.4 T compared to 3 T, due to the use of a surface coil at 3 T. While cell detection limit will be affected by

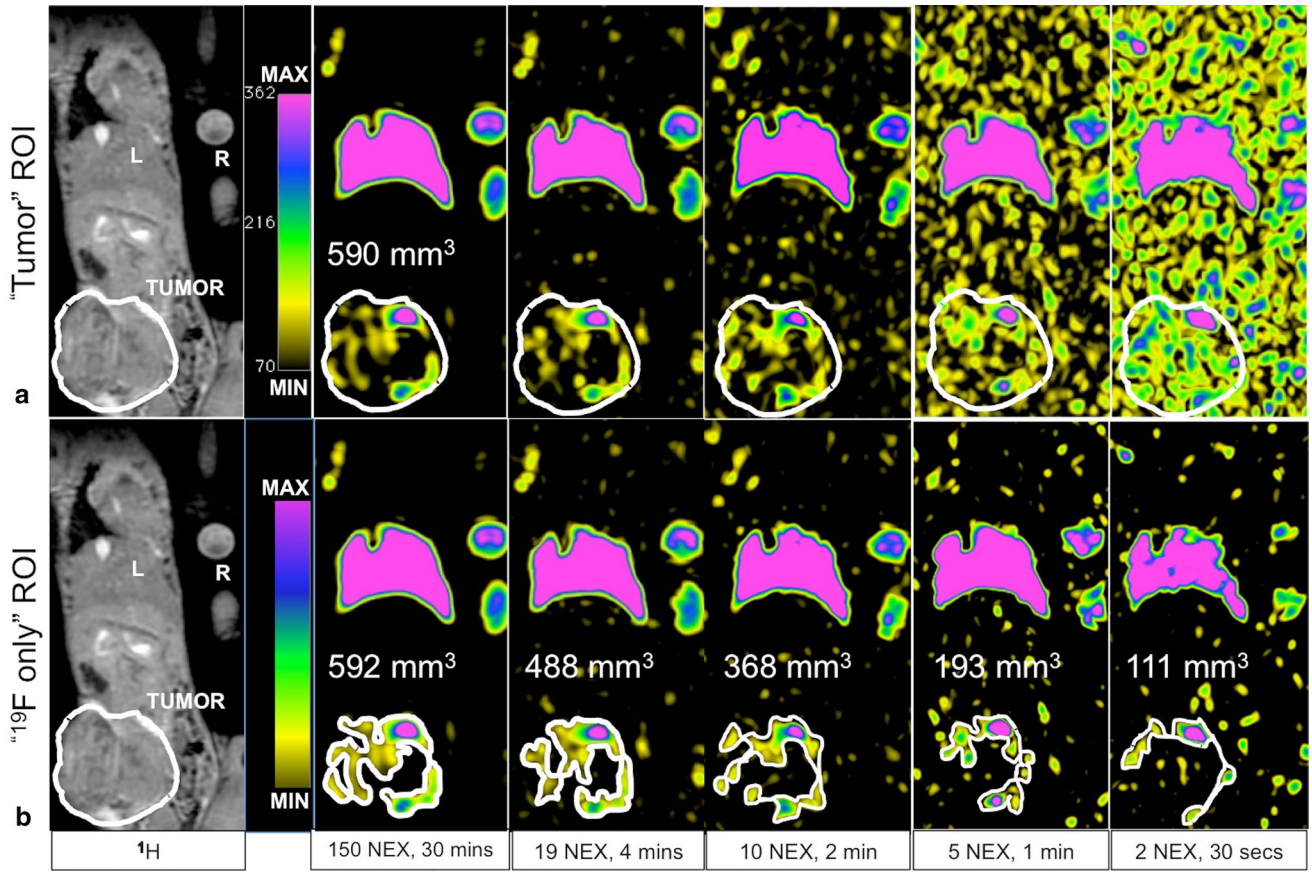

Fig. 5 MRI of a representative 4T1 tumor-bearing mouse at 3 T. ^{1}H images are shown in the far left column. ^{19}F images are shown, with decreasing number of averages (NEX); the values for NEX and scan time are listed along the bottom. **a** Using the "Tumor" ROI method, the tumor is outlined in the proton image and this ROI is used for all ^{19}F images; the volume of the ROI is the same (590 mm^3). Window/level values are the same for all ^{19}F images (min/max: 70/362). **b** Using the "^{19}F only" ROI method, the drawing of the ROI is subjective and depends on ability to see ^{19}F signal. This increases with SNR as does the volume of the ROI selected; volumes are shown above the ROIs. Minimum/maximum signal intensities: 2 NEX: 233/421, 5 NEX: 134/310, 10 NEX: 96/364 and 19 & 150 NEX: 70/362. *L* liver, *R* reference tubes

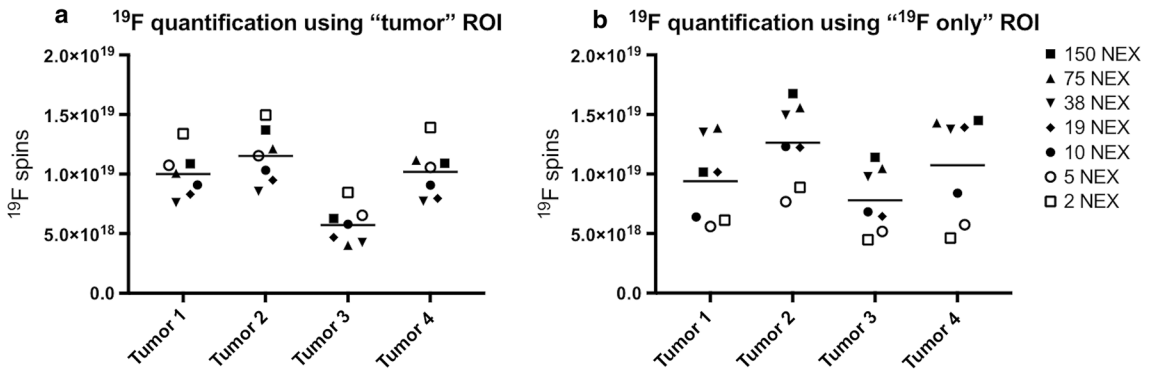

Fig. 6 Scatter plots of ^{19}F spin number for each tumor, quantified using each of the NEX acquisitions by either **a** "tumor" ROI or **b** "^{19}F only" ROI analysis method. The range of ^{19}F spin number is smaller when using a "tumor" ROI versus "^{19}F only" ROI. There is a trend of higher numbers of ^{19}F spins with higher NEX using a "^{19}F only" ROI. Bar is the mean value

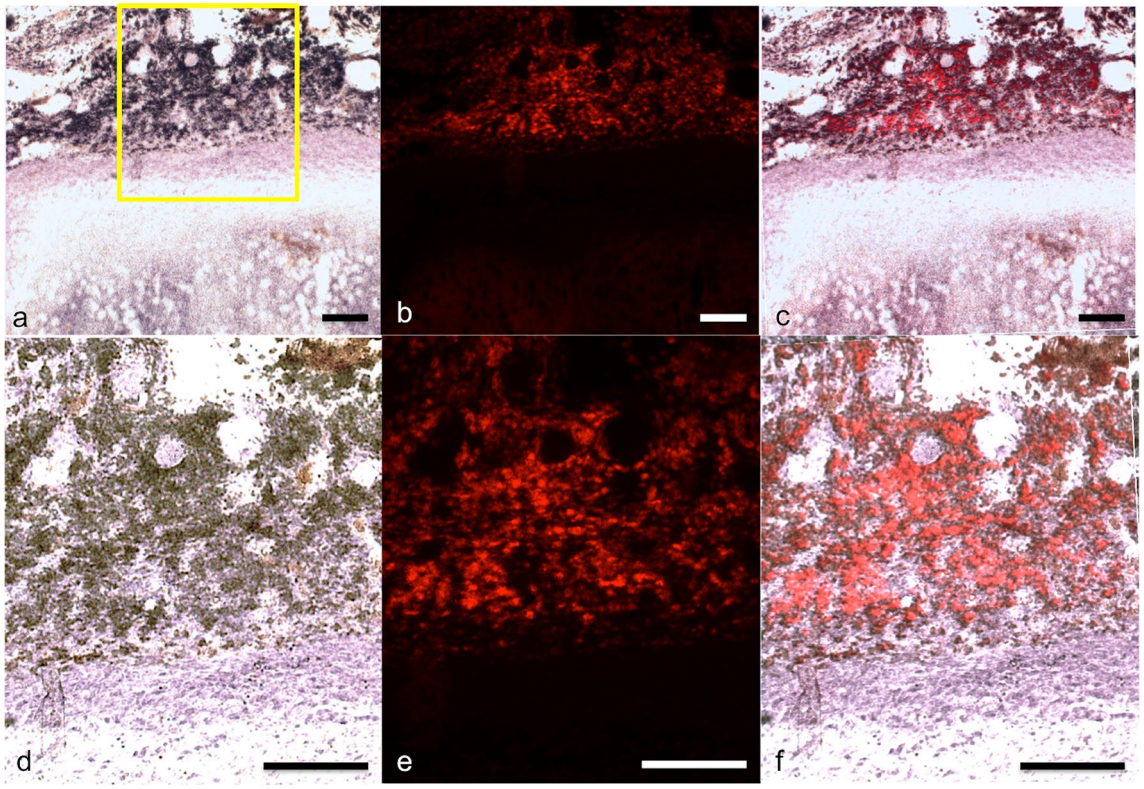

Fig. 7 Microscopy of a tumor 3 weeks post 4T1 cancer cell implantation. **a**, **d** F4/80 DAB stains for macrophages (brown), here evident in the periphery of the tumor. **b**, **e** Red fluorescence from the PFC agent is observed in the same location as the F4/80+ macrophages. The overlay is shown in **c**, **f**. Yellow box in **a** represents the area shown in **d**–**f**. Two magnifications of ×5 (**a**–**c**) and ×10 (**d**–**f**), scale bars represent 200 micron

many factors, including, for example, ^{19}F cell loading, MRI sequence acquisition parameters, type of radiofrequency (RF) coil used and MRI field strength, in this study the different RF coils used at the two field strengths likely played the major role in our ability to detect cells at 3 T. We utilized an in-house built volume birdcage RF coil at 9.4 T, while at 3 T we utilized a commercially built surface coil. Sensitivity and SNR from each coil are dependent on both design and use. For example, we can optimize birdcage coil diameter and length and "filling factor" [37] to improve sensitivity. The birdcage coil we used was built for imaging mice and, therefore, a mouse fits well into the coil (i.e., mouse size dimension equals coil dimension). Surface coils provide superior sensitivity versus volume coils and this is because of a smaller coil diameter and proximity to the region of interest [38]. These coils were both built to maximize sensitivity, with respect to their configurations and use, but it is impossible to compare the two considering their inherent differences.

Our study and others have demonstrated that ^{19}F signal is related to PFC-positive TAMs identified by microscopy [4, 5, 7, 27]. If we use the number of ^{19}F spins/cell measured from the NMR of macrophages labeled in vitro, we can estimate that we are detecting roughly $30–55 \times 10^6$ PFC-labeled cells in the 4T1 tumors only imaged at 3 T. Since cells labeled in vitro will have a higher ^{19}F loading per cell, compared with cells labeled by an IV injection of PFC, this is likely an underestimation.

^{19}F quantification is typically performed using manual delineation of only the perceived ^{19}F signal, with ^{1}H images used for anatomical reference ("^{19}F only" ROI) [2, 3, 27]. However, the distribution of TAMs within a tumor may be sparse and heterogeneous; this has been observed by both clinical histological examination [18, 39] and with preclinical ^{19}F MRI [5, 7]. This, along with low SNR data, will cause regions of ^{19}F signal to be less obvious and may lead to user bias with respect to the ROI chosen for ^{19}F quantification. Here, we used two different methods for ^{19}F quantification. When "^{19}F only" ROI was utilized, a wider range of values for the number of ^{19}F spins was found between the low and high NEX acquisitions and there was a trend of higher numbers of ^{19}F spins measured as NEX/SNR increased. We observed that in low SNR ^{19}F images, when choosing the "^{19}F only" ROI, the size of the ROI was smaller. When using the "tumor" ROI, there was more consistent ^{19}F spin quantification between low versus high SNR ^{19}F images. This

method may produce more consistent results in vivo, as the ROI is taken from an anatomical image and not from perceived ^{19}F signal. However, in ^{19}F images where the signal is obvious and localized to a homogeneous area, ROI can be taken from the ^{19}F data, such as what we have done for the images of PFC-labeled cell pellets.

The ^{19}F MRI methods described could also be adopted for use in other disease models. Not only could an IV injection of a PFC agent label monocyte/macrophage populations in situ to quantify inflammatory responses, but also, for example, ^{19}F MRI could track and quantify a specific, in vitro PFC-labeled cell population, over time. This would be of use in cellular therapy, where ^{19}F MRI could assess the location and success of migration. This has been implemented by Ahrens et al. to study PFC-labeled dendritic cells (DCs), which were introduced into colorectal adenocarcinoma patients as an immunotherapy in a clinical trial [34]. In this instance, they were able to image and quantify the PFC-labeled DCs at the injection site and noted a large decrease in ^{19}F signal at 24 h, which they attribute to DC migration to lymph nodes, or cell death resulting in clearance of the PFC. For future clinical translation of our work, the surface coil utilized in our study was built to image small regions on a human patient and is available commercially. A surface coil like this would be useful for imaging a superficial tumor to study TAMs or a lymph node for immunotherapy studies to confirm successful migration.

Despite strong evidence for a link between TAM content in breast cancer and patient outcome, there are few strategies for measuring TAMs in breast tumors and currently no in vivo approach. With continued developments of this imaging technology on clinical MRI systems, ^{19}F MRI cell tracking has the potential to be used routinely to provide a picture of TAM distribution and a measure of TAM density in breast tumors; this information can be used in a meaningful way to predict response to therapy and monitor treatment.

Acknowledgements We acknowledge the following sources of funding for AVM: Natural Sciences and Engineering Research Council, Molecular Imaging Graduate Program (Western University), Translational Breast Cancer Research Unit, Cancer Research and Technology Transfer Program and Canadian Cancer Society.

Author contributions AVM study conception and design, acquisition of data, analysis and interpretation of data, drafting of manuscript and critical revision. PJF study conception and design, drafting of manuscript and critical revision.

Funding This study was funded by: Canadian Institute for Health Research.

Compliance with ethical standards

Conflict of interest The authors declare that they have no conflict of interest.

Ethical approval All procedures performed in studies involving animals were in accordance with the ethical standards of the institution or practice at which the studies were conducted.

References

1. Balducci A, Helfer BM, Ahrens ET, O'Hanlon CF 3rd, Wesa AK (2012) Visualizing arthritic inflammation and therapeutic response by fluorine-19 magnetic resonance imaging (^{19}F MRI). J Inflamm (Lond) 9:24
2. Shin SH, Kadayakkara DK, Bulte JWM (2017) In vivo (19)F MR imaging cell tracking of inflammatory macrophages and site-specific development of colitis-associated dysplasia. Radiology 282:194–201
3. Zhong J, Narsinh K, Morel PA, Xu H, Ahrens ET (2015) In vivo quantification of inflammation in experimental autoimmune encephalomyelitis rats using fluorine-19 magnetic resonance imaging reveals immune cell recruitment outside the nervous system. PLoS One 10:e0140238
4. Makela AV, Gaudet JM, Foster PJ (2017) Quantifying tumor associated macrophages in breast cancer: a comparison of iron and fluorine-based MRI cell tracking. Sci Rep 7:42109
5. Makela AV, Foster PJ (2018) Imaging macrophage distribution and density in mammary tumors and lung metastases using fluorine-19 MRI cell tracking. Magn Reson Med 80:1138–1147
6. Khurana A, Chapelin F, Xu H, Acevedo JR, Molinolo A, Nguyen Q, Ahrens ET (2018) Visualization of macrophage recruitment in head and neck carcinoma model using fluorine-19 magnetic resonance imaging. Magn Reson Med 79:1972–1980
7. Shin SH, Park SH, Kang SH, Kim SW, Kim M, Kim D (2017) Fluorine-19 magnetic resonance imaging and positron emission tomography of tumor-associated macrophages and tumor metabolism. Contrast Media Mol Imaging 2017:4896310
8. Srinivas M, Boehm-Sturm P, Figdor CG, de Vries IJ, Hoehn M (2012) Labeling cells for in vivo tracking using (19)F MRI. Biomaterials 33:8830–8840
9. Taylor AJ, Granwehr J, Lesbats C, Krupa JL, Six JS, Pavlovskaya GE, Thomas NR, Auer DP, Meersmann T, Faas HM (2016) Probe-specific procedure to estimate sensitivity and detection limits for ^{19}F magnetic resonance imaging. PLoS One 11:e0163704
10. Temme S, Grapentin C, Quast C, Jacoby C, Grandoch M, Ding Z, Owenier C, Mayenfels F, Fischer JW, Schubert R, Schrader J, Flogel U (2015) Noninvasive imaging of early venous thrombosis by ^{19}F magnetic resonance imaging with targeted perfluorocarbon nanoemulsions. Circulation 131:1405–1414
11. Ebner B, Behm P, Jacoby C, Burghoff S, French BA, Schrader J, Flogel U (2010) Early assessment of pulmonary inflammation by ^{19}F MRI in vivo. Circ Cardiovasc Imaging 3:202–210
12. Hitchens TK, Ye Q, Eytan DF, Janjic JM, Ahrens ET, Ho C (2011) ^{19}F MRI detection of acute allograft rejection with in vivo perfluorocarbon labeling of immune cells. Magn Reson Med 65:1144–1153
13. Flögel U, Su S, Kreideweiß I, Ding Z, Galbarz L, Fu J, Jacoby C, Witzke O, Schrader J (2011) Noninvasive detection of graft rejection by in vivo ^{19}F MRI in the early stage. Am J Transplant 11:235–244
14. Srinivas M, Morel PA, Ernst LA, Laidlaw DH, Ahrens ET (2007) Fluorine-19 MRI for visualization and quantification of cell migration in a diabetes model. Magn Reson Med 58:725–734
15. Gaudet JM, Ribot EJ, Chen Y, Gilbert KM, Foster PJ (2015) Tracking the fate of stem cell implants with fluorine-19 MRI. PLoS One 10:e0118544

16. Tiainen S, Tumelius R, Rilla K, Hämäläinen K, Tammi M, Tammi R, Kosma VM, Oikari S, Auvinen P (2015) High numbers of macrophages, especially M2-like (CD163-positive), correlate with hyaluronan accumulation and poor outcome in breast cancer. Histopathology 66:873–883
17. Yuan Z-Y, Luo R-Z, Peng R-J, Wang S-S, Xue C (2014) High infiltration of tumor-associated macrophages in triple-negative breast cancer is associated with a higher risk of distant metastasis. Onco Targets Ther 7:1475–1480
18. Gwak JM, Jang MH, Il Kim D, Seo AN, Park SY (2015) Prognostic value of tumor-associated macrophages according to histologic locations and hormone receptor status in breast cancer. PLoS One 10:1–14
19. Reigstad I, Smeland HYH, Skogstrand T, Sortland K, Schmid MC, Reed RK, Stuhr L (2016) Stromal integrin α11β1 affects RM11 prostate and 4T1 breast xenograft tumors differently. PLoS One 11:e0151663
20. Wong CW, Song C, Grimes MM, Fu W, Dewhirst MW, Muschel RJ, Al-Mehdi A-B (2002) Intravascular location of breast cancer cells after spontaneous metastasis to the lung. Am J Pathol 161:749–753
21. Gudbjartsson H, Patz S (1995) The rician distribution of noisy MRI data. Magn Reson Med 34:910–914
22. Wu YL, Ye Q, Foley LM, Hitchens TK, Sato K, Williams JB, Ho C (2006) In situ labeling of immune cells with iron oxide particles: an approach to detect organ rejection by cellular MRI. Proc Natl Acad Sci USA 103:1852–1857
23. Zarif L, Postel M, Trevino L, Riess JG, Valla A, Follana R (1994) Biodistribution and excretion of a mixed fluorocarbon-hydrocarbon "dowel" emulsion as determined by 19F NMR. Artif Cells Blood Substit Immobil Biotechnol 22:1193–1198
24. Ahrens ET, Zhong J (2013) In vivo MRI cell tracking using perfluorocarbon probes and fluorine-19 detection. NMR Biomed 26:860–871
25. Wang Y-XJ (2011) Superparamagnetic iron oxide based MRI contrast agents: current status of clinical application. Quant Imaging Med Surg 1:35–40
26. Gustafson HH, Holt-Casper D, Grainger DW, Ghandehari H (2015) Nanoparticle uptake: the phagocyte problem. Nano Today 10:487–510
27. Khurana A, Chapelin F, Xu H, Acevedo JR, Molinolo A, Nguyen Q, Ahrens ET (2017) Visualization of macrophage recruitment in head and neck carcinoma model using fluorine-19 magnetic resonance imaging. Magn Reson Med 79:1972–1980
28. Weibel S, Basse-Luesebrink TC, Hess M, Hofmann E, Seubert C, Langbein-Laugwitz J, Gentschev I, Sturm VJF, Ye Y, Kampf T, Jakob PM, Szalay AA (2013) Imaging of intratumoral inflammation during oncolytic virotherapy of tumors by 19F-magnetic resonance imaging (MRI). PLoS One 8:e56317
29. Balducci A, Wen Y, Zhang Y, Helfer BM, Hitchens TK, Meng WS, Wesa AK, Janjic JM (2013) A novel probe for the non-invasive detection of tumor-associated inflammation. Oncoimmunology 2:e23034
30. Daldrup-Link HE, Golovko D, Ruffell B, Denardo DG, Castaneda R, Ansari C, Rao J, Tikhomirov GA, Wendland MF, Corot C, Coussens LM (2011) MRI of tumor-associated macrophages with clinically applicable iron oxide nanoparticles. Clin Cancer Res 17:5695–5704
31. Shi Q, Pisani LJ, Lee YK, Messing S, Ansari C, Bhaumik S, Lowery L, Lee BD, Meyer DE, Daldrup-Link HE (2013) Evaluation of the novel USPIO GEH121333 for MR imaging of cancer immune responses. Contrast Media Mol Imaging 8:281–288
32. Leimgruber A, Berger C, Cortez-Retamozo V, Etzrodt M, Newton AP, Waterman P, Figueiredo JL, Kohler RH, Elpek N, Mempel TR, Swirski FK, Nahrendorf M, Weissleder R, Pittet MJ (2009) Behavior of endogenous tumor-associated macrophages assessed in vivo using a functionalized nanoparticle. Neoplasia 11:459-IN4
33. Ahrens ET, Young W-B, Xu H, Pusateri LK (2011) Rapid quantification of inflammation in tissue samples using perfluorocarbon emulsion and fluorine-19 nuclear magnetic resonance. Biotechniques 50:229–234
34. Ahrens ET, Helfer BM, O'Hanlon CF, Schirda C (2014) Clinical cell therapy imaging using a perfluorocarbon tracer and fluorine-19 MRI. Magn Reson Med 72:1696–1701
35. Gocheva V, Wang H-W, Gadea BB, Shree T, Hunter KE, Garfall AL, Berman T, Joyce JA (2010) IL-4 induces cathepsin protease activity in tumor-associated macrophages to promote cancer growth and invasion. Genes Dev 24:241–255
36. Wyckoff JB, Wang Y, Lin EY, Li JF, Goswami S, Stanley ER, Segall JE, Pollard JW, Condeelis J (2007) Direct visualization of macrophage-assisted tumor cell intravasation in mammary tumors. Cancer Res 67:2649–2656
37. Hill HDW, Richards RE (1968) Limits of measurement in magnetic resonance. J Phys E 1:977
38. Haase A, Odoj F, Von Kienlin M, Warnking J, Fidler F, Weisser A, Nittka M, Rommel E, Lanz T, Kalusche B, Griswold M (2000) NMR probeheads for in vivo applications. Concepts Magn Reson 12:361–388
39. Morita Y, Zhang R, Leslie M, Adhikari S, Hasan N, Chervoneva I, Rui H, Tanaka T (2017) Pathologic evaluation of tumor-associated macrophage density and vessel inflammation in invasive breast carcinomas. Oncol Lett 14:2111–2118